IIETA International Information and Engineering Technology Association
Advancing the World of Information and Engineering

Journal Européen des Systèmes Automatisés
Vol. 59, No. 10, October, 2026, pp. 3055-3065
Journal homepage: http://iieta.org/journals/jesa

IoT-Based Embedded Climate Control and Priority-Based Photovoltaic–Battery–Grid Energy Management for Black Soldier Fly Bioconversion of Canteen Fruit and Vegetable Waste

Reza Rahmadian[1*], Alfarid Hendro Yuwono[1], Firman Yasa Utama[1], I Gde Agung Sri Sidhimantra[1], Suprapto[1], Anggi Rahmad Zulfikar[1], Rachman Widohardhono[1], Deshinta Arrova Dewi[2], Aliyu Sabo[3], Elok Rosyida Proposalia[4]

[1] Faculty of Vocational Studies, Universitas Negeri Surabaya, Kota Surabaya 60231, Indonesia
[2] Faculty of Data Science and Information Technology, INTI International University, Putra Nilai 71800, Malaysia
[3] Department of Electrical and Electronic Engineering, Nigerian Defence Academy, Kaduna PMB 2109, Nigeria
[4] Faculty of Engineering, Universitas Negeri Surabaya, Kota Surabaya 60231, Indonesia

Corresponding Author Email: rezarahmadian@unesa.ac.id

Copyright: ©2026 The authors. This article is published by IIETA and is licensed under the CC BY 4.0 license (http://creativecommons.org/licenses/by/4.0/).

https://doi.org/10.18280/jesa.591024

Received: 6 August 2026
Revised: 12 October 2026
Accepted: 24 October 2026
Available online: 31 October 2026

Keywords:
black soldier fly, embedded control, energy management strategy food production, photovoltaic, Internet of Things, load prioritization, organic waste bioconversion

ABSTRACT

Small black soldier fly (BSF) bioconversion units often stop because feeding is irregular and their climate actuators depend on an unreliable grid. This study presents an automated rearing system built around an ESP32 controller with a DHT22 sensor, hysteresis control of heating, ventilation, and humidification, cloud telemetry, and a priority-based energy management strategy (EMS) for a photovoltaic (PV)–battery–grid supply that reserves a battery band for the monitoring loads during grid outages. Canteen fruit and vegetable waste (FVW) served as the application case. Bench tests verified sensing, relay switching, remote override, and cloud synchronization; closed-loop climate performance has not yet been tested. Hourly simulations showed that a 200 Wp array with a 100 Ah battery covers 86–94% of the 0.60–0.78 kWh day^{-1} demand (5th percentile 69% in a 400-run Monte Carlo analysis). The EMS gave almost the same renewable fraction (RF) as a single-threshold controller in normal operation, but in a simulated overcast–outage sequence it kept the monitoring loads supplied while the single-threshold controller lost them for 18 h. Two manual cycles associated feed shortage with a 92.1% fall in egg-normalized yield, and a five-day feeding trial gave 91.3 ± 9.2% apparent substrate disappearance. Metered field validation of the complete system remains necessary.

1. INTRODUCTION

Wasted food is one of the largest and least valorized fractions of urban solid waste. Global estimates place municipal solid waste above 2 billion tonnes per year, with food and green residues dominating in developing economies [1], and food discarded by households, food services and retailers at about 931 million tonnes per year [2]. A university canteen is a compact version of the same problem: its residues are separable at the source, arrive at predictable times and are generated next to engineering staff who can operate and instrument a treatment unit.

Larvae of the black soldier fly (BSF), Hermetia illucens, are among the most studied biological agents for such streams [3, 4]. They consume fruit and vegetable waste (FVW), reduce its mass and store protein and fat that can partly replace fishmeal and soybean meal in feed [5], and when the process is properly operated it emits less greenhouse gas than composting [6]. Fruit and vegetable substrates typically lose 60–75% of their mass [7, 8], and pre-consumer food wastes 37–79% [9]. The performance, however, depends strongly on the feeding rate [10], the substrate [11-13] and the microclimate, notably temperature [14, 15] and humidity [16].

In Indonesia, more than 60% of municipal solid waste is organic, and BSF units are now run by communities, hospitals and campuses [17, 18]. Field experience shows that these units fail mostly for operational reasons. A community facility in Padang worked at 20–25% of capacity with an irregular 5–10 kg day^{-1} supply until a formal agreement with food businesses was signed, after which it processed 6,156 kg in two months [17]; interrupted feeding is also known to slow larval development [19]. Reviews of BSF treatment chains conclude that pre-processing, a continuous larval supply, and process control decide whether laboratory results can be repeated in practice [20-22].

From the viewpoint of automated systems, a small rearing unit is an embedded control and power-supply problem: the controller must keep temperature and relative humidity (RH) within the larval range, report the process state to the operators, and remain operational when the electrical supply fails. Internet of Things (IoT) nodes that measure temperature and humidity and switch heaters, fans, or humidifiers have been reported for BSF rearing [23-26], and vision-based larval monitoring is emerging [27]. These systems are usually

supplied from the grid and do not consider what happens to the controller and telemetry during outages. Energy is not a minor issue: a containerized BSF module treating 719 kg of food waste per day consumed 162 kWh day^{-1}, and climate control was its second-largest environmental burden after drying [28], whereas a 15 t day^{-1} plant reached 17.4 kg CO_2-eq per tonne treated [29]. Hybrid renewable systems with rule-based energy management are mature in rural electrification [30, 31], but these lines of work have not been combined for insect bioconversion units, whose loads differ in criticality: losing heating for a few hours is tolerable in the tropics, whereas losing the controller and telemetry hides overheating, fermentation or missed feeding.

This paper addresses that gap for the canteen of the Faculty of Vocational Studies, Universitas Negeri Surabaya (UNESA). The contribution is mainly in the automated system, with the bioconversion process used as the application case and as the basis for specifying the system: (i) an ESP32-based incubator node in which local hysteresis control, cloud telemetry and remote override are assigned to explicitly defined layers, verified at component level on the bench; (ii) a four-tier photovoltaic (PV)–battery–grid energy management strategy (EMS) with an islanding reserve for the monitoring loads, evaluated by hourly simulation, outage stress tests and Monte Carlo uncertainty analysis; and (iii) process indicators from two manual production cycles and a standardized feeding trial, which define the feeding requirement that the system has to support. The work covers prototype functional verification and energy simulation; it does not yet include field validation of the complete closed-loop system. Section 2 reviews related work, Section 3 describes the materials, system design, and methods, Section 4 presents and discusses the results, and Section 5 concludes.

2. RELATED WORK

2.1 Bioconversion performance and process requirements

Bioconversion performance is usually reported with the bioconversion rate (BCR, biomass produced per unit substrate), the substrate reduction, the waste reduction index and the efficiency of conversion of digested feed [7, 32]. For fruit, vegetable and food wastes at 32 ± 3 °C, substrate reduction of 60–67% and BCR of 4.8–5.7% have been measured [7]; fruit byproducts reached 73–75% reduction [8]; catering, municipal, slaughter and manure-based streams show large differences in growth and conversion [32, 33]. Larvae grow fastest near 27–30 °C and survive poorly at the extremes [14, 15], while about 70% RH favours hatching and emergence [16]. From these studies, an automated unit must provide two things: a microclimate near 27–33 °C and 60–70% RH, and a feed supply matched to the larval intake [10, 19].

2.2 Embedded monitoring and control for insect rearing

Relay-based on–off control with hysteresis remains the standard for heaters and humidifiers because it is robust and cheap, and a dead band prevents chattering [34]; model-based controllers improve tracking but need a plant model and tuning that a small enclosure rarely justifies. Reported BSF IoT nodes include an IoT and computer-vision incubator [24], an IoT-controlled egg cycle [25] and ESP8266 sensor networks [26], reviewed in [23]. These nodes demonstrate sensing, actuation and remote dashboards, but they are grid-supplied, they evaluate egg or larval output rather than the behaviour of the controller, and they do not state which functions remain available when the network or the power supply fails.

2.3 Hybrid supply and energy management for small loads

Rule-based EMS for hybrid systems are preferred in small installations because they need no forecast and run on low-cost controllers [30, 31], and limiting the depth of discharge prolongs lead-acid battery life [35]. In rural electrification, these strategies already rank loads and shed the least important ones first.

2.4 Research gap and comparison criteria

Table 1 compares representative studies against seven criteria (C1–C7, defined in the table caption). A criterion is marked only when the cited work implements it and reports a quantitative evaluation. Two gaps follow. First, none of the BSF automation studies [23-26, 28] combines a hybrid supply with load priorities, so none specifies how the controller and telemetry are protected during outages, while the EMS literature [30, 31] has not been applied to bioprocess loads of different criticality. Second, feeding continuity has been examined only in feeding-rate experiments with a controlled supply [10] and in a community facility report [17]; none of the automation studies treats the feed supply as a monitored variable, although interrupted feeding slows development [19]. The present work addresses the first gap as its main engineering contribution and uses the second to define the operating requirements of the system.

Table 1. Comparison with related studies

Study	C1	C2	C3	C4	C5	C6	C7
Magee et al. [10]	–	–	–	✓	–	–	–
Yuwono et al. [14]; Musyaddad et al. [15]	✓[a]	–	–	–	–	–	–
Huang et al. [24]; Kuncoro et al. [25]; Efendi et al. [26]	✓	✓	–	–	–	–	–
Efendi et al. [28]	✓	–	✓	–	–	–	✓
Yuwono et al. [17]	–	–	✓	✓	–	–	–
Zulkarnain [30]; Yang et al. [31]	–	–	–	–	✓	✓	✓
This work	✓	✓	✓	✓	✓	✓	✓

Note: ✓ = implemented and quantitatively evaluated; – = not addressed; [a] fixed laboratory chamber; C1 = automatic climate control of the rearing space; C2 = cloud telemetry; C3 = substrate pre-processing; C4 = feed-supply analysis; C5 = hybrid renewable supply with storage; C6 = load-priority energy management; C7 = energy or emission indicator.

3. MATERIALS AND METHODS

3.1 Research site and design workflow

The unit was built at the Organic Waste Process Laboratory and the Kanvanesa canteen of the Faculty of Vocational Studies, UNESA, Surabaya (about 7.3 °S, 112.7 °E). The canteen separates fruit and vegetable residues at the source, about 4 kg per operating day, which are kept in three labelled 60 L bins and shredded before feeding by a 250 W, six-blade shredder with a 4 L chamber and a 5 mm screen. The research followed a design-build-verify cycle: production records were

analysed, a feeding protocol was standardized, the embedded node was designed and bench-tested, and the hybrid supply was sized and evaluated by simulation.

3.2 Electrical architecture

Figure 1 shows the electrical architecture. A 200 Wp array (2 × 100 Wp) charges a 12 V, 100 Ah valve-regulated lead-acid battery through a 12 V/12 A solar charge controller. The battery feeds a 12 V direct-current (DC) bus that supplies the controller, sensors, display, relays, and fans directly; a DC–DC boost converter produces 24 V for the ultrasonic mist makers; and an inverter generates 220 V alternating current (AC) for the heating lamps and the shredder. A relay source selector connects the AC loads either to the inverter or to the grid of the state electricity company (Perusahaan Listrik Negara, PLN). The ESP32 measures the battery voltage and current to estimate the state of charge (SOC), selects the source of each load group and exchanges data with the cloud.

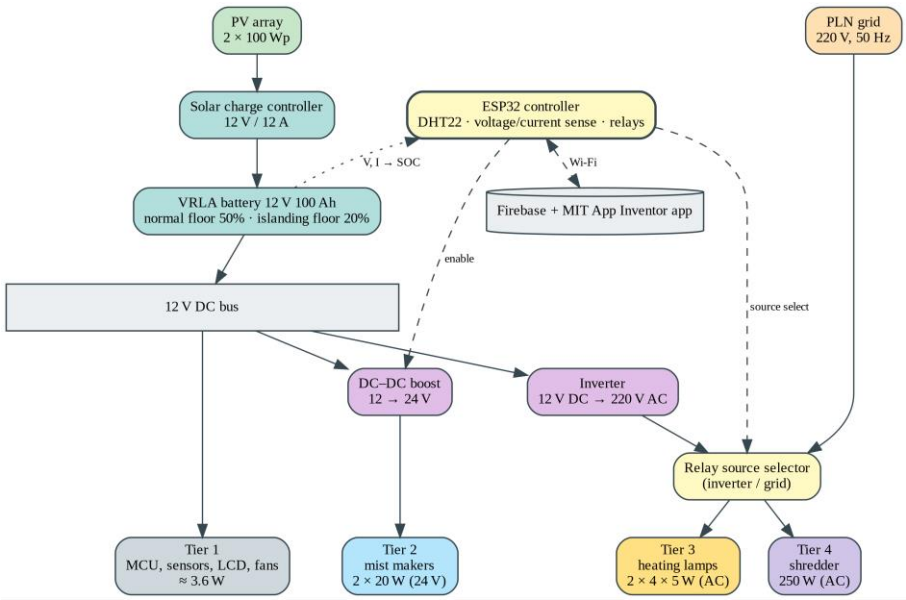


Figure 1. Electrical architecture of the photovoltaic (PV)–battery–grid supply with direct-current (DC) and alternating-current (AC) buses, the four load tiers and the data links

Note: SOC = state of charge; VRLA = valve-regulated lead-acid; PLN = state electricity company.

3.3 Production records and standardized feeding trial

Two manual cycles, carried out before the IoT node was available, provided the baseline. Both were reared on the laboratory rack under ambient conditions without climate control, and no continuous temperature or humidity record exists for either cycle. Cycle 1 started in September 2024 from 1 g of eggs and received canteen waste 12 times; at harvest, 90% of the pupae were collected and 10% were kept for adult emergence. Cycle 2 started on 1 April 2025 from 4 g of eggs and was fed only on larval days 4 and 5, against the laboratory operating procedure of about 15 feedings per month at roughly 1 kg day^{-1}; the reduction was caused by an irregular canteen supply and limited operator availability. Cycle 2 was followed until larval day 30, by which time no adults had emerged. The indicators use whole-cycle totals, so they do not depend on the exact harvest day. Besides egg input and feeding, the April report notes that the containers had been reorganized by developmental stage on a tiered rack, and the season differed (dry season in September, end of the wet season in April); these differences are compared in Section 4.1. Egg mass, each feed portion and total pupal biomass were recorded on verified log sheets. Harvest quality was checked with the laboratory's routine quality-control sampling, in which sampling units taken from the harvested pupae are weighed as groups. Because the number of pupae in a unit was not part of this routine record, the unit mass is used here only as a relative quality index against the laboratory standard, not as an individual pupal mass. The 4.0 g reference is the internal harvest-quality standard of the Organic Waste Process Laboratory, derived from its earlier production records rather than from the literature. Ten units were weighed individually in Cycle 2, whereas the Cycle 1 log sheet records only the mean unit mass. With M_f the wet feed, M_p the pupal biomass and M_e the egg mass, the indicators in Eqs. (1) and (2) were computed: BCR on a wet basis, the egg-normalized feeding density (EFD) and the egg-normalized yield (EY).

$$\mathrm{BCR} = \frac{M_p}{M_f} \times 100\% \tag{1}$$

$$\mathrm{EFD} = \frac{M_f}{M_e}, \mathrm{EY} = \frac{M_p}{M_e} \tag{2}$$

The standardized feeding trial was then run with two parallel rearing boxes (10 L containers, 18 cm deep), each holding about 1 kg of larvae from the same cohort in the active feeding phase, i.e., within the 6–26-day feeding window of the laboratory protocol; the larval density estimated in Section 4.2 (about 55–110 mg per larva) is consistent with this stage. Each box received 2 kg of shredded substrate at 08:00 on five consecutive days under laboratory ambient conditions. The substrate came mainly from the canteen; during the project, waste from a second campus food court was used when the canteen supply was short, so its composition could vary between days. Its moisture was adjusted before feeding to avoid compaction. The offered mass M_0 was weighed at the feeding time t_0; the box was inspected periodically, and when

no further visible consumption occurred (or the substrate was depleted) the time t_h was noted and the remaining substrate M_t was weighed. Larvae and frass were not separated from the residue before weighing, and no larva-free control box was included to quantify evaporation and microbial decomposition. The quantities in Eqs. (3) and (4) are therefore an apparent substrate disappearance and an apparent rate, not a measured larval ingestion. The number of larvae per box was estimated by dividing the daily intake by literature feeding rates of 100–200 mg larva^{-1} day^{-1} [7, 10].

$$\eta_c = \frac{M_0 - M_t}{M_0} \times 100\% \quad (3)$$

$$r = \frac{M_0 - M_t}{t_h - t_0} \quad (4)$$

3.4 Embedded node, control laws and data flow

Each incubator is a plywood enclosure of 63 × 45 × 30 cm. The node consists of an ESP32 microcontroller, a DHT22 temperature–humidity sensor with a stated accuracy of ±0.5 °C and ±2–5% RH [36], a 16 × 2 liquid-crystal display on an Inter-Integrated Circuit (I²C) bus, four 5 W lamps for heating, two 5 V fans for ventilation and a 24 V ultrasonic mist maker, all switched by relay modules (Table 2, Figure 2). Measurements and actuator states are pushed to Google Firebase over Wi-Fi, and an MIT App Inventor application provides authenticated access, live readings for two boxes and manual override.



Figure 2. Embedded node hardware: (a) enclosure assembly, (b) firmware bench test, (c) two-box mobile dashboard and (d) enclosure drawing

Table 2. Electrical ratings of the incubator node per incubator

Component	Qty	Rating	Function	Bus/Tier
ESP32 DevKit	1	≈ 0.5–0.8 W	Control, Wi-Fi	12 V DC/Tier 1
DHT22 (AM2302)	1	3.3–5 V, < 2 mA	T and RH sensing	12 V DC/Tier 1
LCD 16 × 2 + I²C, relays	1 + 3	≈ 0.5 W	Display, switching	12 V DC/Tier 1
DC fan	2	5 V, ≈ 1 W each	Ventilation	12 V DC/Tier 1
Ultrasonic mist maker	1	24 V, ≈ 20 W	Humidification	24 V DC/Tier 2
Incandescent lamp	4	220 V, 5 W each	Heating	AC/Tier 3
Shredder (shared)	1	220 V, 250 W	Pre-processing	AC/Tier 4

Note: DC = direct current; AC = alternating current; RH = relative humidity; LCD = liquid-crystal display; I²C = inter-integrated circuit bus.

The heater state u_h and the humidifier state u_m follow the hysteresis laws in Eqs. (5) and (6), where T is the measured temperature, RH the relative humidity and k the sampling instant. The fans are switched on above 36 °C. The set points were chosen from the larval temperature optimum [14, 15] and the 70% humidity optimum [16]; the 10-point dead band in Eq. (6) replaces the single 60% threshold of the first firmware and prevents relay chattering [34].

$$u_h(k) = 1 \; if \; T < 30\,°C; 0 \; if \; T \geq 32\,°C; \; u_h(k-1) otherwise \quad (5)$$

$$u_m(k) = 1 \text{ if } RH < 60\%; 0 \; if \; RH \geq 70\%; \; u_m(k-1) otherwise \quad (6)$$

Table 3 summarizes how the sensor readings are used. All control decisions are taken locally by the ESP32 in every loop: it reads the DHT22, evaluates Eqs. (5) and (6) and the fan threshold, estimates the SOC from the battery voltage and current, and executes the tier and source decisions of Algorithm 1. Firebase is only a communication and storage layer: the node publishes temperature, RH, SOC and relay states and reads a manual override flag and set-point changes written by the mobile application, which is a supervisory interface and never closes a control loop. Loss of Wi-Fi or of the Firebase connection therefore does not stop heating, ventilation, humidification or load management; only remote override and cloud logging are unavailable until the connection is restored. Network loss therefore affects supervision, not control.

Table 3. Allocation of functions between the embedded controller, the cloud database and the mobile application

Layer	Inputs	Decisions and Outputs	Without Network
ESP32	T, RH; battery V and I; grid status	Eqs. (5)–(6), fan rule; SOC; Algorithm 1; relays	Unchanged (local)
Firebase	Node data; override flag; set points	Stores and relays data; no control logic	No data stored
Mobile app	Firebase data; login	Display; manual override; set points	No live data or commands

Note: RH = relative humidity; SOC = state of charge; T = temperature; V = voltage; I = current.

3.5 Priority-based energy management and simulation

The loads are grouped into four priority tiers: Tier 1 contains the controller, sensors, display, relays and fans (about 3.6 W for two incubators); Tier 2 the mist makers; Tier 3 the heating lamps; and Tier 4 the deferrable shredder. Three strategies were compared: S0, grid only; S1, a conventional solar home system in which PV is used first and the battery supplies all loads down to a single 50% SOC disconnect before the grid takes over, with the shredder run at 08:00; and S2, the proposed tiered EMS described by Algorithm 1. In S2 the shredder is shifted to the PV peak at 11:00, the battery is normally cycled between 100% and 50% SOC to protect the lead-acid cells [35], and the band from 50% to 20% SOC is reserved for Tier 1 when the grid fails.

Algorithm 1. Tiered EMS executed every control interval Δt

Input: P_pv, SOC, grid_ok, demands D1..D4 of Tiers 1–4
1: avail ← P_{pv}
2: for i = 1 to 4 do ▷ serve tiers in priority order
3: use ← min(avail, Di); avail ← avail − use; Di ← Di − use
4: floor ← 0.50
5: if i = 1 and not grid_ok then floor ← 0.20 ▷ islanding reserve
6: if i = 4 then floor ← 0.80 ▷ shredder only on surplus
7: if Di > 0 and SOC > floor then discharge battery for Di
8: if Di > 0 and grid_ok then supply Di from grid via selector
9: if Di > 0 and not grid_ok then shed tier i (Tier 1 logged as unserved)
10: end for
11: charge battery with avail (curtail if SOC = 100%)
12: publish T, RH, SOC and relay states to Firebase

The hourly energy balance uses Eq. (7) for the PV output and Eq. (8) for the battery energy. P_{STC} is the array rating, $G(t)$ the plane-of-array irradiance, G_{STC} = 1,000 W m^{-2}, the performance ratio (PR) accounts for system losses and $P_{cc,max}$ the charge-controller limit; E_b is the stored energy, P_{ch} and P_{dis} the charging and discharging powers and η_{ch}, η_{dis} their efficiencies. $G(t)$ was a half-sine profile between 06:00 and 18:00 whose integral equals the peak sun hours (PSH) obtained from the NASA POWER database [37].

$$P_{pv}(t) = \min\{P_{STC} \cdot \frac{G(t)}{G_{STC}} \cdot PR, P_{cc,max}\} \quad (7)$$

$$E_b(t+1) = E_b(t) + \eta_{ch} P_{ch}(t)\Delta t - \frac{P_{dis}(t)\Delta t}{\eta_{dis}} \quad (8)$$

The heating duty was obtained from a steady envelope balance, $d_h = \min\{1, UA(T_{set} - T_{amb})/P_{lamp}\}$, with UA = 4.6 W K^{-1} for the 1.22 m² plywood envelope; neglecting the metabolic heat of the larvae makes this estimate conservative. Mist-maker duty was proportional to the RH deficit below 65%, and converter losses of the boost stage are covered by the ±25% uncertainty assigned to the mist-maker power. Performance was expressed by the renewable fraction (RF), the specific energy consumption (SEC), the energy intensity per kilogram of larvae (EBI) and the avoided emissions in Eqs. (9) and (10), where E_{grid} and E_{load} are the daily grid and load energies, M_w and M_L the daily waste input and larval output, and EF the grid emission factor of the Java–Madura–Bali system [38]. Table 4 lists all parameters.

$$RF = 1 - \frac{E_{grid}}{E_{load}}, SEC = \frac{E_{load}}{M_w}, EBI = \frac{E_{load}}{M_L} \quad (9)$$

$$m_{CO_2} = EF \cdot (E_{load} - E_{grid}) \quad (10)$$

Each case was run for ten identical days and the last day was reported. Resilience was tested with a 4 h evening outage on ten consecutive nights and with a sequence of one clear day, three overcast days (1.5 PSH) and one clear day with a 6 h outage (00:00–06:00) every night. The unserved Tier 1 energy was the sum of the hourly shortfalls of Tier 1 demand, and the loss-of-load hours (LOLH) were the number of hourly steps in which any part of the Tier 1 demand could not be supplied. A Monte Carlo analysis (N = 400 per season, S2) sampled UA (±30%), PR (0.70–0.85), mist-maker power (±25%), controller power (−20% to +50%) and PSH (±15%) from uniform distributions, and Spearman rank coefficients ranked the drivers of RF. All energy results in this paper are simulation outputs; none of them were metered on the installed PV and battery system [39].

Table 4. Simulation parameters

Parameter	Value	Parameter	Value
Incubators/envelope UA	2/4.6 W K^{-1}	PV array/PR	200 Wp/0.78
Heater set point	30 °C (2 K hysteresis)	Charge controller	12 V, 12 A
Dry season T/RH	24.5–33.5 °C/52–82%	Battery	12 V, 100 Ah VRLA
Wet season T/RH	25.0–31.0 °C/68–90%	SOC floors (normal/islanding)	50%/20%
PSH dry/wet [37]	5.6/4.2 kWh m^{-2} d^{-1}	η_{ch}, η_{dis}, η_{inv}	0.85/0.95/0.90
Shredder use	250 W × 0.2 h d^{-1}	EF (Java–Madura–Bali grid) [38]	0.87 kg CO$_2$ kWh^{-1}
Waste/larvae per day	4.0 kg/0.20 kg	Tariff (R-1)	IDR 1,444.70 kWh^{-1}

Note: PV = photovoltaic; PR = performance ratio; RH = relative humidity; PSH = peak sun hours; SOC = state of charge; VRLA = valve-regulated lead-acid; EF = emission factor.

3.6 Statistical analysis

Data are reported as mean ± standard deviation (SD). For the Cycle 2 harvest the statistical unit was the sampling unit (n = 10); normality was checked with the Shapiro–Wilk test and the mean was compared with the 4.0 g standard by a one-sample t-test with Cohen's d. Cycle 1 (mean only) could not be tested, and the cycles (n = 1 each) were compared descriptively. In the feeding trial the unit was the box-day (5 per box). Because the days of a box are repeated measurements of one larval population and the two boxes are not replicated production cycles, Welch's t-test and a paired t-test with day as the pairing factor are reported only to describe the between-box difference. The association between daily disappearance and feeding interval was described by Pearson's r on the ten box-days with a 95% confidence interval (CI) and by a repeated-measures (within-box) correlation. Results with $p > 0.05$ are reported as non-significant tendencies. Analyses used Python 3 with SciPy.

4. RESULTS AND DISCUSSION

4.1 Feed supply in the manual cycles: An observational comparison

Table 5 and Figure 3 compare the two manual cycles. Cycle 1 turned 10.41 kg of waste into 1.12 kg of pupae with a mean unit mass of 4.1 g, just above the 4.0 g standard. Cycle 2 began with four times more eggs but received only 2.20 kg of feed in two portions. Feed mass fell by 78.9% and pupal biomass by 68.2%; relative to the installed biological capacity, EFD dropped by 94.7% (10,412 to 550 g g^{-1}) and EY by 92.1% (1,121 to 89 g g^{-1}). The log also records that no adults emerged on days 27–30, which agrees with delayed development under food deprivation [10, 19].

Table 5. Rearing conditions and production indicators of the two manual cycles

Item	Cycle 1 (Sep. 2024)	Cycle 2 (Apr. 2025)	Change
Observation end	Harvest; 10% kept for breeding	Day 30; no emergence	–
Rearing environment	Ambient rack; no T/RH log	Ambient rack; no T/RH log	Season differed
Egg input (g)	1.0	4.0	+300%
Feeding events	12	2 (days 4 and 5)	−83.3%
Feed Mf (g)	10,412	2,200	−78.9%
Pupal biomass Mp (g)	1,121	356	−68.2%
BCR, Eq. (1) (%)	10.8	16.2	+5.4 pp
EFD, Eq. (2) (g g^{-1})	10,412	550	−94.7%
EY, Eq. (2) (g g^{-1})	1,121	89	−92.1%
Unit mass (g), n units	4.1 (mean only)	1.57 ± 0.53, n = 10	−61.7%

Note: BCR = bioconversion rate; EFD = egg-normalized feeding density; EY = egg-normalized yield; T = temperature; RH = relative humidity; pp = percentage points. Each cycle is a single run; changes are descriptive.

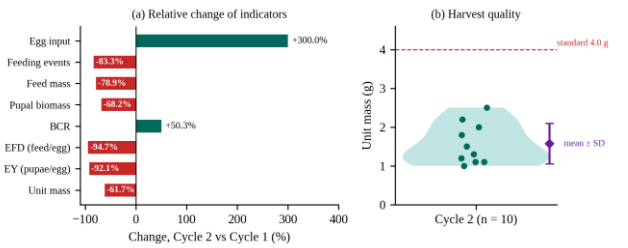


Figure 3. Manual-cycle diagnostics: (a) relative change of production indicators from Cycle 1 to Cycle 2 and (b) distribution of Cycle 2 sampling-unit masses against the 4.0 g laboratory standard

Note: BCR = bioconversion rate; EFD = egg-normalized feeding density; EY = egg-normalized yield.

The rise of BCR from 10.8% to 16.2% is counter-intuitive. Under severe restriction, the larvae eat almost all of the little substrate offered, so the biomass-to-feed ratio rises while total yield and individual mass collapse. BCR therefore rewards starvation, whereas EFD and EY, which relate feed and yield to the installed biological capacity, reveal the deficit. The ten Cycle 2 units averaged 1.57 ± 0.53 g (95% CI 1.19–1.95 g; Shapiro–Wilk $p = 0.24$), far below the standard ($t(9) = -14.64$, $p < 0.001$, $d = -4.63$), with a coefficient of variation of 33.4% that is consistent with uneven access to food. This comparison is observational. The two cycles are single runs that differed in egg input, feeding frequency and season, and neither has a temperature or humidity record, so the data establish an association between feed shortage and the poorer harvest, not a causal effect. Feed shortage is the most plausible explanation because the feed per gram of eggs fell by a factor of about 19 while the other recorded conditions stayed the same, and because the operating log attributes the shortfall to the missed feedings; however, a higher larval density from the larger egg input and seasonal effects cannot be separated from it. For the automated system, this result defines a requirement rather than a proof: the feeding events must be logged and checked against the installed egg mass. The design response was therefore a 180 L source buffer, a fixed collection schedule, shredding and a feeding log in the dashboard.

4.2 Short-term consumption in the standardized feeding trial

Of the 20 kg offered during the five-day trial, 18.25 kg disappeared, giving 91.3 ± 9.2% apparent substrate disappearance (Table 6, Figure 4). Box 1 lost 1,840 ± 207 g day^{-1} at 189 ± 73 g h^{-1} and Box 2 1,810 ± 182 g day^{-1} at 165 ± 35 g h^{-1}. The difference between the boxes was small in absolute terms (30 g day^{-1}; Welch $p = 0.81$, paired $p = 0.83$), but with two boxes and five days per box this only shows that the two boxes behaved similarly during this period; it does not establish that the procedure is reproducible over repeated production cycles. Because residues were weighed together with frass and without an evaporation control, part of the disappearance may be moisture loss and decomposition rather than ingestion, so the 91.3% value is an upper bound for larval consumption. The pooled rate of 177 ± 56 g h^{-1} lies in the 150–200 g h^{-1} band adopted as an operating baseline.

Table 6. Feeding-trial statistics

Variable	Box 1	Box 2	Pooled	Welch p / Paired p
Daily disappearance C (g day^{-1})	1,840 ± 207	1,810 ± 182	1,825 ± 184	0.81 / 0.83
Apparent disappearance η_c (%)	92.0 ± 10.4	90.5 ± 9.1	91.3 ± 9.2	0.81 / 0.83
Feeding interval $t_h - t_0$ (h)	10.6 ± 3.0	11.2 ± 1.3	10.9 ± 2.2	0.70 / 0.77
Apparent rate r (g h^{-1})	189 ± 73	165 ± 35	177 ± 56	0.53 / 0.63

Note: M_0 = 2,000 g box^{-1} day^{-1}; statistical unit = box-day, n = 5 per box; tests are descriptive because the five days within a box are not independent and only two boxes were used.

Daily disappearance tended to decrease as the feeding interval became longer (pooled $r = -0.63$, 95% CI −0.90 to 0.00, $p = 0.052$; within-box $r = -0.62$, $p = 0.072$; Figure 4 (c)). Neither correlation reaches the 0.05 level, so the relation is a tendency. It is also partly built into the measurement, because the interval ends when consumption stops. Descriptively, portions cleared within 7–10 h were eaten completely, whereas 200–500 g remained when the interval stretched to 11–14 h (Figure 4(a)). The 2 kg portion appears close to the intake capacity of a box, about 1.8 kg day^{-1}, and splitting it into two

feedings (for example 1.2 kg at 08:00 and 0.8 kg at 14:00) may reduce residues and fermentation; this has to be tested. With 100–200 mg larva^{-1} day^{-1} [7, 10], the measured intake corresponds to roughly 9,000–18,000 larvae per box, or a mean larval mass of about 55–110 mg for the roughly 1 kg of larvae in each box, which is plausible for larvae in the active feeding phase. Daily disappearance is not equivalent to end-of-cycle substrate reduction (60–75% for fruit and vegetable substrates [7, 8]), because the final residue includes frass, but it is a convenient same-day indicator that the node can log: rates persistently below 150 g h^{-1} indicate overfeeding or stress, and rates above 250 g h^{-1} underfeeding. These thresholds are provisional and are based only on the five days reported here.

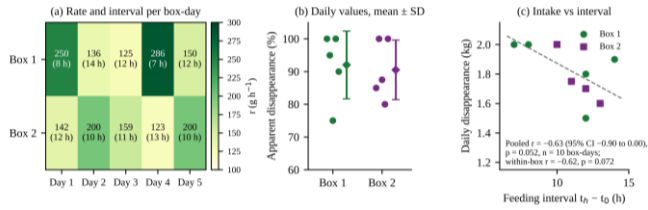


Figure 4. Standardized feeding trial: (a) apparent consumption rate and feeding interval for each box-day, (b) daily apparent disappearance per box with mean ± standard deviation (SD) and (c) daily disappearance against feeding interval with pooled and within-box correlations

4.3 Functional verification of the embedded node

Table 7 summarizes the bench tests. All modules communicated correctly; the relays followed both the automatic laws in Eqs. (5) and (6) and manual commands from the application, and readings of the two boxes were synchronized with Firebase. A reading of 29.3 °C and 66.6% RH was displayed during the test, inside the target band. These were component-level pass/fail checks. No continuous temperature or humidity record was logged during the bench tests, so the response of the enclosure after an actuator switches on, and hence the closed-loop control performance (settling time, overshoot, switching frequency, spread around the set points), has not yet been verified. The enclosure has been fabricated and the electronics are being installed; a 72 h logging test of the installed node is the first item of the next stage (Section 4.5).

Table 7. Bench functional verification of the embedded node (component-level tests)

Test Item	Expected Behaviour	Observed Result
DHT22 acquisition and LCD	Stable T and RH readings	Pass (29.3 °C, 66.6% RH)
Heater and fan logic, Eq. (5)	Lamp ON < 30 °C, OFF ≥ 32 °C; fans ON > 36 °C	Pass (auto and manual)
Humidifier logic, Eq. (6)	Mist ON < 60% RH, OFF ≥ 70% RH	Pass
Firebase telemetry and app control	Per-box values; relays follow remote commands	Pass (Box 1 and Box 2)
User access	Authenticated dashboard login	Pass
Closed-loop response	T and RH return to band after actuation	Not yet tested

Note: LCD = liquid-crystal display; RH = relative humidity.

4.4 Simulated energy performance of the hybrid supply

The simulated demand is 0.78 kWh day^{-1} in the dry season and 0.60 kWh day^{-1} in the wet season (Table 8, Figure 5(a)). In the dry season the mist makers take 31% of the energy (245 Wh day^{-1}) because the midday humidity falls below 60%, while in the wet season humidification is unnecessary and heating dominates (460 Wh day^{-1}, 77%). Tier 1 needs only 86–92 Wh day^{-1}. On a simulated dry day under S2 (Figure 5(b)) the battery carries the night load to the 50% floor near 05:00, the grid covers about two hours, and the array then supplies all loads and recharges the battery.

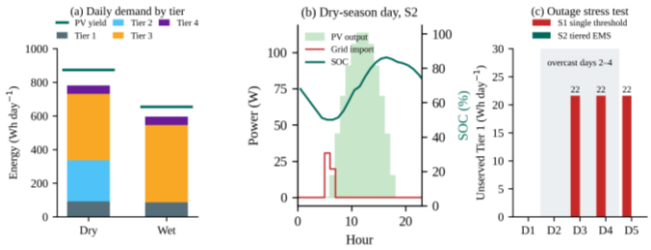


Figure 5. Simulated hybrid supply results: (a) daily demand by load tier with photovoltaic (PV) yield, (b) PV output, grid import and state of charge (SOC) on a dry-season day under S2, and (c) unserved Tier 1 energy per day in the overcast–outage stress test

Table 8. Simulated daily energy results for a 200 Wp array and a 100 Ah battery

Season	Strategy	E_{load} (Wh)	E_{pv} (Wh)	E_{grid} (Wh)	RF (%)	Unserved Tier 1, Stress Test (Wh)
Dry	S0 grid only	782	–	782	0.0	144 [a]
Dry	S1 single threshold	782	874	51	93.5	–
Dry	S2 tiered EMS	782	874	51	93.5	–
Wet	S0 grid only	596	–	596	0.0	144 [a]
Wet	S1 single threshold	596	655	86	85.5	64.8 [b] (LOLH 18 h)
Wet	S2 tiered EMS	596	655	82	86.3	0 [b] (LOLH 0 h)

Note: [a]ten nights with a 4 h evening outage; [b]overcast–outage sequence (three overcast days, 6 h outage every night). PV = photovoltaic; RF = renewable fraction; LOLH = loss-of-load hours; EMS = energy management strategy. All values are hourly simulation results.

In the simulation, the array covers 93.5% of demand in the dry season and 85.5–86.3% in the wet season, limiting grid import to 51–86 Wh day^{-1}. Under normal operation S1 and S2 give the same RF in the dry season and differ by only 0.8 percentage points in the wet season, a gain that comes from moving the shredder to the PV peak. The tiered EMS therefore does not increase everyday solar utilization appreciably; its contribution is reliability of the critical loads during outages, and the two effects should not be confused. With ten nightly 4 h outages, the grid-only case lost its monitoring loads for 40 h (144 Wh), while both battery-backed strategies kept them alive. In the overcast–outage sequence, S1 reached its 50%

disconnect point before the night outages of days 3–5 and lost all loads, including the controller and telemetry. The 18 h value is the count of hourly steps with unserved Tier 1 demand: 6 h on each of three nights. At the 3.6 W Tier 1 demand this equals 64.8 Wh (21.6 Wh per night, Figure 5 (c)). It is a loss-of-load figure for the monitoring tier, not an energy saving. S2 shed heating and humidification but kept Tier 1 supplied from the islanding reserve with zero LOLH. At an average Tier 1 demand of 3.6 W, the 50–20% band corresponds to about 95 h of autonomous monitoring, which matters because a short loss of heating is tolerated by larvae in the tropics while a loss of monitoring hides overheating, fermentation or missed feeding.

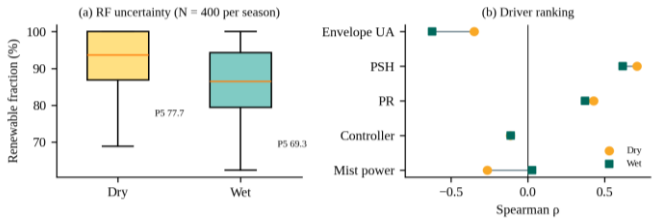


Figure 6. Monte Carlo analysis of the simulated S2 strategy: (a) renewable-fraction distribution per season and (b) Spearman rank correlation of the renewable fraction with the uncertain parameters

Two limitations of the model matter here. First, the solar profile is an idealized half-sine scaled to monthly PSH and the loads use steady duty cycles, so cloud transients, longer rainy spells, start-up currents, and inverter standby losses are not represented. Second, the hourly step averages power within each hour: outages shorter than one hour, minute-scale SOC dips during actuator start-up and switching within the hour are not resolved, and LOLH is quantized to whole hours, so the 18 h figure is uncertain by up to about one hour per outage event. The main conclusion is nevertheless robust, because the 30% reserve band (about 340 Wh after discharge losses) is about 16 times the Tier 1 energy of a 6 h outage, whereas S1 has no reserve once its single threshold is reached. Absolute RF values and outage durations still require metering.

Figure 6 shows that parametric uncertainty does not overturn these findings. The mean RF is 92.0% in the dry season (5th–95th percentile 77.7–100%) and 86.2% in the wet season (69.3–100%), with daily demand of 697–869 Wh and 494–668 Wh. Irradiance (ρ = 0.62–0.71) and PR (ρ = 0.37–0.43) are the main positive drivers; the envelope *UA* is the strongest negative driver in the wet season ($\rho = -0.62$), when heating dominates, while the mist-maker power matters only in the dry season ($\rho = -0.26$). For the rainy months, better insulation of the enclosure is therefore as effective as additional PV capacity.

4.5 Benchmarking, limitations and next tests

Table 9 places the results among published systems. The Cycle 1 BCR of 10.8% (pupae, wet) exceeds the 4.8–5.7% reported on a larval-gain basis for fruit, vegetable and food waste [7] and approaches the 12.8% wet larvae-to-feed ratio of a containerized module [28]; the bases differ, so the comparison is indicative. The simulated SEC of 0.15–0.20 kWh kg^{-1} is below the 0.23 kWh kg^{-1} of the containerized module [28] because the tropical climate removes most heating and no drying stage is included, although per kilogram of fresh larvae the present unit (3.0–3.9 kWh kg^{-1}) needs about twice as much energy (1.8 kWh kg^{-1}), reflecting the lower productivity of small trays. Operational electricity of a grid-only unit would emit about 150 kg CO_2 t^{-1} of waste; with the hybrid supply and S2 this falls to about 14 kg CO_2 t^{-1}, the same order as the 17.4 kg CO_2-eq t^{-1} of a 15 t day^{-1} plant [29], a full life-cycle value against an operational one.

Table 9. Benchmarking against published black soldier fly (BSF) bioconversion systems

Study	Scale/Substrate	Climate	Conversion	Energy/Carbon
Mertenat et al. [7]	Lab; fruit, vegetable, food waste	32 ± 3 °C	SR 60–67%; BCR 4.8–5.7%	n.r.
Karthikeyani et al. [8]	Lab; fruit byproducts	Controlled	SR 73–75%	n.r.
Scieuzo et al. [9]	Lab; pre-consumer food wastes	28 °C, 70% RH	Reduction 37–79%	n.r.
Efendi et al. [28]	Container; 719 kg d^{-1}	26 °C, 66% RH	Wet BCR 12.8%	0.23 kWh kg^{-1}; 2.77 kg CO_2-eq kg^{-1} dry larvae
Guo et al. [29]	Plant; 15 t d^{-1}	Industrial	Material flow analysis	17.4 kg CO_2-eq t^{-1} (life-cycle)
This work	Canteen; FVW 4 kg d^{-1}	30–32 °C, 60–70% RH	BCR 10.8–16.2%; apparent disappearance 91.3%	0.15–0.20 kWh kg^{-1}; ≈ 14 kg CO_2 t^{-1} (simulated)

Note: n.r. = not reported; SR = substrate reduction; BCR = bioconversion rate; RH = relative humidity; FVW = fruit and vegetable waste.

The engineering limitations are as follows: the node has passed component-level bench tests only; the DHT22 has not been calibrated against a reference instrument; all energy results are hourly simulations without metering; the SOC estimate and islanding logic have not been tested with a real grid interruption; and the process baseline rests on two unreplicated cycles and a five-day, two-box trial without an evaporation control. The next stage comprises, in order of priority, a 72-h closed-loop logging test of the installed node with a calibrated reference thermohygrometer (settling time, overshoot, switching frequency); metering of PV, battery and grid energy for at least one month with deliberate grid interruptions, including network-loss tests of the telemetry chain; and replicated incubator cycles against an open-rack control with frass separation and a larva-free control. NH_3 and CO_2 sensing, vision-based larval sizing [24, 27], and a forecast-based EMS will follow.

5. CONCLUSIONS

This paper presented an automated rearing system for BSF bioconversion of canteen waste at UNESA, consisting of an ESP32 node with local hysteresis control, cloud telemetry and remote override, powered by a PV–battery–grid supply with a priority-based EMS. The control decisions are taken locally,

so a network outage interrupts supervision but not control. Bench tests confirmed sensing, relay switching, remote commands and cloud synchronization at the component level. Hourly simulation indicated that a 200 Wp array with a 100 Ah battery covers 86–94% of the 0.60–0.78 kWh day^{-1} demand, remaining above 69% in 95% of Monte Carlo cases. The tiered EMS hardly changed the RF under normal operation, but in a simulated overcast–outage sequence it kept the monitoring loads supplied, whereas a single-threshold controller lost them for 18 h. As the application case, two manual cycles showed that a feed shortage was associated with a 92.1% fall in egg-normalized yield although the BCR increased, so egg-normalized indicators are proposed for logging, and a five-day trial gave 91.3% apparent substrate disappearance with 2 kg box^{-1} day^{-1} close to the intake capacity.

These results are a prototype functional verification and an energy simulation, not a field validation of the complete closed-loop system. Closed-loop temperature and humidity performance, sensor calibration, the metered energy balance, the islanding reserve under real grid interruptions and the reproducibility of the feeding protocol remain to be demonstrated, beginning with a 72 h closed-loop logging test and a month of metered operation with deliberate grid interruptions.

ACKNOWLEDGMENT

This research was funded by the Institute for Research and Community Service (LPPM), Universitas Negeri Surabaya, under the University Assignment Research scheme 2025. The authors thank Kanvanesa (Kantin Vokasi UNESA) and Mrs. Lilis Sulandari for supplying the organic waste, and Binar A'ian Chariza and the Lowproc team of the Organic Waste Process Laboratory for daily rearing, feeding and data recording.

REFERENCES

[1] Goh, K.C., Kurniawan, T.A., Meidiana, C., et al. (2026). Hospital waste management in Germany and the European Union during the Industry 5.0 era for carbon neutrality by 2050: A critical review. Waste Management & Research: The Journal for a Sustainable Circular Economy, 44(2): 116-132. https://doi.org/10.1177/0734242X251361726

[2] Ramajayam, J.G., Govindarajan, M., Lakshmipathy, M.V., et al. (2026). Continuous flow hydroprocessing of waste plastics using ionic liquid catalyst. Scientific Reports, 16(1): 9261. https://doi.org/10.1038/s41598-026-39132-z

[3] United Nations Environment Programme. (2021). Food Waste Index Report 2021. UNEP, Nairobi. https://www.unep.org/resources/report/unep-food-waste-index-report-2021.

[4] Surendra, K.C., Tomberlin, J.K., van Huis, A., Cammack, J.A., Heckmann, L.H.L., Khanal, S.K. (2020). Rethinking organic wastes bioconversion: Evaluating the potential of the black soldier fly (Hermetia illucens (L.)) (Diptera: Stratiomyidae) (BSF). Waste Management, 117: 58-80. https://doi.org/10.1016/j.wasman.2020.07.050

[5] Gold, M., Tomberlin, J.K., Diener, S., Zurbrügg, C., Mathys, A. (2018). Decomposition of biowaste macronutrients, microbes, and chemicals in black soldier fly larval treatment: A review. Waste Management, 82: 302-318. https://doi.org/10.1016/j.wasman.2018.10.022

[6] Barragán-Fonseca, K.B., Dicke, M., van Loon, J.J.A. (2017). Nutritional value of the black soldier fly (Hermetia illucens L.) and its suitability as animal feed – A review. Journal of Insects as Food and Feed, 3(2): 105-120. https://doi.org/10.3920/JIFF2016.0055

[7] Mertenat, A., Diener, S., Zurbrügg, C. (2019). Black soldier fly biowaste treatment – Assessment of global warming potential. Waste Management, 84: 173-181. https://doi.org/10.1016/j.wasman.2018.11.040

[8] Karthikeyani, T., Sivasubramanian, K., Maheswari, M., et al. (2024). The efficiency of black soldier fly larvae with vegetable, fruit and food waste as biological tool for sustainable management of organic waste. International Journal of Environment and Climate Change, 14(2): 441-448. https://doi.org/10.9734/IJECC/2024/v14i23959

[9] Scieuzo, C., Franco, A., Salvia, R., et al. (2023). Enhancement of fruit byproducts through bioconversion by Hermetia illucens (Diptera: Stratiomyidae). Insect Science, 30(4): 991-1010. https://doi.org/10.1111/1744-7917.13155

[10] Magee, K., Halstead, J., Small, R., Young, I. (2021). Valorisation of organic waste by-products using black soldier fly (Hermetia illucens) as a bio-convertor. Sustainability, 13(15): 8345. https://doi.org/10.3390/su13158345

[11] Diener, S., Zurbrügg, C., Tockner, K. (2009). Conversion of organic material by black soldier fly larvae: Establishing optimal feeding rates. Waste Management & Research, 27(6): 603-610. https://doi.org/10.1177/0734242X09103838

[12] Lalander, C., Diener, S., Zurbrügg, C., Vinnerås, B. (2019). Effects of feedstock on larval development and process efficiency in waste treatment with black soldier fly (Hermetia illucens). Journal of Cleaner Production, 208: 211-219. https://doi.org/10.1016/j.jclepro.2018.10.017

[13] Ardita, M., Yuwono, A.H., Kusrahardjo, G., Labib, R.P.M.D., Widodo, K.A. (2024). Preliminary assessment on the performance of long distance wireless data transmission for disaster early warning system. AIP Conference Proceedings, 3077(1): 050067. https://doi.org/10.1063/5.0216537

[14] Yuwono, A.H., Dewi, D.A., Balakrishnan, R., et al. (2026). A portable solar-powered wireless charger: Design, implementation, and performance analysis. Buletin Ilmiah Sarjana Teknik Elektro, 8(3): 824-836. https://doi.org/10.12928/biste.v8i3.15226

[15] Musyaddad Romadoni, A., Agusti Putra, P., Riza Mayora, D., et al. (2025). Toll gate systems with YOLO-CNN based using Raspberry Pi for vehicle class detection. EPJ Web of Conferences, Surabaya, Indonesia, 344: 01010. https://doi.org/10.1051/epjconf/202534401010

[16] Yuwono, A.H., Rivai, M., Sardjono, T.A. (2020). Solar panel-based wireless battery charging system using fuzzy control method. IOP Conference Series: Materials Science and Engineering, 847(1): 012088. https://doi.org/10.1088/1757-899X/847/1/012088

[17] Yuwono, A.H., Widyartono, M., Aziz, A.A.S., et al.

(2026). Self-sustaining embedded edge-vision node for industrial OSH monitoring: Fusing YOLOv8n compliance matrix with active-cooled dual-axis photovoltaic tracking. Buletin Ilmiah Sarjana Teknik Elektro, 8(5): 1590-1602. https://doi.org/10.12928/biste.v8i5.17209

[18] Sakanti, M.M., Efendi, A., Surjanto, A., Falahuddin, M.A., Khakim, N., Kuncoro, C.B.D. (2023). Development of PLC trainer kit as a teaching aid for electric motor practice. In Proceedings of the International Conference on Electrical Engineering, Computer Science and Informatics (EECSI), pp. 467-474. https://doi.org/10.1109/EECSI59885.2023.10295587

[19] Wu, C.M., Chen, S.C., Chen, Y.J., Efendi, A. (2024). A personalized contactless emergency aid system designed for individuals with profound physical disabilities. IEEE Access, 12: 27115-27126. https://doi.org/10.1109/ACCESS.2024.3366068

[20] Isa, I.G.T., Effendi, A. (2024). Deep reinforcement learning in agricultural IoT-based: A review. E3S Web of Conferences, 479: 07004. https://doi.org/10.1051/e3sconf/202447907004

[21] Efendi, A., Nugraha, A., Baharta, R. (2019). Manufacturing of electrical dryer machine for food and fruit products. IOP Conference Series: Materials Science and Engineering, 692(1): 012006. https://doi.org/10.1088/1757-899X/692/1/012006

[22] Purnomo, S., Sofyan, H., Siswanto, I., et al. (2025). Development of cooperative learning by technopreneur for vocational schools-augmented reality model to improve the survival skills. International Journal of Information and Education Technology, 15(9): 1884-1892. https://doi.org/10.18178/ijiet.2025.15.9.2389

[23] Efendi, A., Komarudin, D. (2019). Evaluation of the application of occupational safety and health (OSH) at the Subang State Polytechnic laboratory. Automotive Experiences, 2(1): 9-14. https://doi.org/10.31603/ae.v2i1.2472

[24] Huang, C.Y., Efendi, A., Wang, Y.C. (2026). Curriculum-guided deep reinforcement learning with fuzzy rewards for autonomous push-grasp manipulation in cluttered environments. Robotics and Autonomous Systems, 198: 105325. https://doi.org/10.1016/j.robot.2025.105325

[25] Kuncoro, C.B.D., Efendi, A., Sakanti, M.M. (2023). Wearable sensor for psychological stress monitoring of pregnant woman – State of the art. Measurement, 221: 113556. https://doi.org/10.1016/j.measurement.2023.113556

[26] Efendi, A., Ammarullah, M.I., Isa, I.G.T., et al. (2025). IoT-based elderly health monitoring system using Firebase cloud computing. Health Science Reports, 8(3): e70498. https://doi.org/10.1002/hsr2.70498

[27] Nguyen, T.T.X., Tomberlin, J.K., Vanlaerhoven, S. (2015). Ability of black soldier fly (Diptera: Stratiomyidae) larvae to recycle food waste. Environmental Entomology, 44(2): 406-410. https://doi.org/10.1093/ee/nvv002

[28] Efendi, W. (2025). Behavior collapse investigation of a steel sheet pile with LISA FEA V8. SAINSTECH NUSANTARA, 2(2): 53-64. https://doi.org/10.71225/jstn.v2i2.110

[29] Wirawan, W., Zulkarnain, A., Utomo, I.S., Rouf, M.S., Azari, M.A.B., Prasetijo, J. (2024). Modeling and simulation of static strength railway bogie bolster using Ansys Workbench. SAINSTECH NUSANTARA, 1(4): 21-29. https://doi.org/10.71225/jstn.v1i4.54

[30] Zulkarnain, A., Damayanti, A.T., Saputro, R.Y. (2024). Effect of groove shape in GTAW welding on bending strength of aluminium 6061. SAINSTECH NUSANTARA, 1(4): 30-39. https://doi.org/10.71225/jstn.v1i4.74

[31] Yang, G., Chiau, L., Jiadong, W. (2024). Automation of trolley wire adjustment to improve safety of deviation maintenance on Japanese type catenary networks. SAINSTECH NUSANTARA, 1(2): 17-28. https://doi.org/10.71225/jstn.v1i2.53

[32] Zulkarnain, A., Rianta, W., Pradana, A.F. (2024). A comparative study of Mobilith SHC 100 and Gulf Crown EP 2 greases on the train wheel bearings. SAINSTECH NUSANTARA, 1(1): 13-20. https://doi.org/10.71225/jstn.v1i1.41

[33] Girsang, A.S., Kaburuan, E.R., Peranginangin, E., Kristianto, K., Lambert, R.V., Yunanda, R. (2024). Black soldier fly (BSF) farming in egg cycle based on IoT technology. AIP Conference Proceedings, 2867: 030022. https://doi.org/10.1063/5.0225243

[34] Syifa, F.T., Hikmaturokhman, A., Qisthani, N.N., Fitriana, G.F., Arifin, M. (2024). Implementation of sensor node and ESP8266-based network in black soldier fly (BSF) cultivation to support circular economy. In 2024 IEEE International Conference on Artificial Intelligence and Mechatronics Systems (AIMS), Bandung, Indonesia, pp. 1-6. https://doi.org/10.1109/AIMS61812.2024.10513124

[35] Manduca, G., Wilson, L.T., Stefanini, C., Romano, D. (2025). Automated detection of larval stages of the black soldier fly (Hermetia illucens Linnaeus) through deep learning augmented with optical flow. Information Processing in Agriculture, 12(4): 501-510. https://doi.org/10.1016/j.inpa.2025.05.001

[36] Liu, T. (2024). Digital-output relative humidity & temperature sensor/module DHT22 (DHT22 also named as AM2302). Product datasheet. Aosong Electronics Co., Ltd., Guangzhou, China. https://www.sparkfun.com/datasheets/Sensors/Temperature/DHT22.pdf.

[37] NASA Langley Research Center. (n.d.). POWER Data Access Viewer – Prediction of Worldwide Energy Resources. Monthly climatology for 7.3° S, 112.7° E (Surabaya, Indonesia). https://power.larc.nasa.gov/data-access-viewer/.

[38] Efendi, A., Wirawan, W.A., Nugroho, A., et al. (2026). AI-driven tactile sensing and force measurement for surgical robotic manipulation: A systematic review with a metrological perspective. Measurement, 123904. https://doi.org/10.1016/j.measurement.2026.123904

[39] Yuwono, A.H., Afandi, A.N., Fadlika, I. (2026). An integrated IoT-based smart farming system for off-season Hylocereus undatus cultivation: Dual-axis solar tracking with active cooling and precision LED light. In 2026 Ninth International Conference on Vocational Education and Electrical Engineering (ICVEE), Surabaya, Indonesia, pp. 722-729. https://doi.org/10.1109/ICVEE71133.2026.11766274

NOMENCLATURE

C	daily apparent substrate disappearance, g day^{-1}
d_h	heating duty, –
E_b	battery energy, Wh
E_{grid}, E_{load}, E_{pv}	daily grid, load and PV energy, Wh
EF	grid emission factor, kg CO_2 kWh^{-1}
G, G_{STC}	irradiance and its value at standard test conditions, W m^{-2}
M_0, M_t	offered and remaining substrate mass, g
M_e, M_f, M_p	egg, feed and pupal mass, g
M_w, M_L	daily waste input and larval output, kg
m_{CO2}	avoided emissions, kg CO_2
P_{STC}, $P_{cc,max}$	array rating and charge-controller limit, W
P_{ch}, P_{dis}	battery charging and discharging power, W
r	apparent consumption rate, g h^{-1}
T, RH	temperature, °C; relative humidity, %
t_0, t_h	feeding time and end-of-consumption time, h
u_h, u_m	heater and humidifier relay states, –
UA	envelope heat-loss coefficient, W K^{-1}

Greek symbols

η_c	apparent substrate disappearance, %
η_{ch}, η_{dis}, η_{inv}	charging, discharging and inverter efficiency, –

Subscripts

BCR	bioconversion rate, %
EBI	energy per kilogram of larvae, kWh kg^{-1}
EFD, EY	egg-normalized feeding density and yield, g g^{-1}
PR	performance ratio, –
RF, SEC	renewable fraction, %; specific energy consumption, kWh kg^{-1}s